

Analytical approach to directed sandpile models on the Apollonian networkAndré P. Vieira,¹ José S. Andrade, Jr.,^{2,3} Hans J. Herrmann,^{2,3} and Roberto F. S. Andrade⁴¹*Departamento de Engenharia Metalúrgica e de Materiais, Universidade Federal do Ceará, Campus do Pici, 60455-760 Fortaleza, Brazil*²*Departamento de Física, Universidade Federal do Ceará, Campus do Pici, 60455-760 Fortaleza, Brazil*³*Computational Physics, IfB, ETH-Hönggerberg, Schafmattstrasse 6, 8093 Zürich, Switzerland*⁴*Instituto de Física, Universidade Federal da Bahia, 40210-340 Salvador, Brazil*

(Received 29 January 2007; published 21 August 2007)

We investigate a set of directed sandpile models on the Apollonian network, which are inspired by the work of Dhar and Ramaswamy [Phys. Rev. Lett. **63**, 1659 (1989)] on Euclidian lattices. They are characterized by a single parameter q , which restricts the number of neighbors receiving grains from a toppling node. Due to the geometry of the network, two- and three-point correlation functions are amenable to exact treatment, leading to analytical results for avalanche distributions in the limit of an infinite system for $q=1, 2$. The exact recurrence expressions for the correlation functions are numerically iterated to obtain results for finite-size systems when larger values of q are considered. Finally, a detailed description of the local flux properties is provided by a multifractal scaling analysis.

DOI: [10.1103/PhysRevE.76.026111](https://doi.org/10.1103/PhysRevE.76.026111)

PACS number(s): 05.65.+b, 89.75.-k, 45.70.Vn

I. INTRODUCTION

The interaction networks of many real systems with a large number of basic units are often found to display power-law distributions of node degrees and small-world properties [1,2]. Examples stem from many different areas, such as electric power distribution, food webs in ecology, information flow in the internet, interaction among financial institutions, and so on [3,4]. In recent years, complex networks have also attracted attention as alternative topological structures to ordered Euclidian lattices, on which many physical models can be defined. These structures offer a suitable scenario to mimic the effect of geometry in real systems and have already been used in the investigation of the properties of magnetic [5–7] and electron [8] systems.

Understanding the stability of complex networks becomes of relevance for the management of natural and human-built systems, as it can provide guidelines to avoid an irreversible collapse and to enhance the robustness of their structure. Another issue that deserves attention is the occurrence of events that may cause permanent or temporary damage to the network, which can be interpreted as avalanches within the proposed self-organized criticality (SOC) scenario [9]. It is well known that a typical signature of SOC systems is the possibility of the occurrence of a very large avalanche that can extend itself over the whole network, causing its breakdown. Specific sandpile models defined on complex networks have been recently investigated [10], as well as models where the network is not fixed, but the set of connections evolves slowly with time [11]. In the first case, avalanches refer to the motion of mass units from one node to its neighbors, while in the last approach avalanches refer to bursts of rewiring connections among the network nodes. Also noteworthy are the recent attempts to use SOC concepts with respect to brain activity, both in Euclidian and scale-free networks [12–14].

It is well known that directed models, like the one proposed by Dhar and Ramaswamy [15], constitute one of the few classes of SOC models that can be exactly solved on Euclidian lattices. This is essentially related to their Abelian property, according to which the effect of two successive grain additions on the lattice does not depend on their order. In the context of complex networks, the Apollonian packing problem [16] inspired the introduction of the so-called Apollonian network [17,18]. Besides displaying both scale-free and small-world features, the hierarchical geometry of this network enables the derivation of tractable analytical expressions for a variety of equilibrium and dynamical models [19]. This leads either to exact results or to recurrence relations that can be numerically iterated.

In this work, we analyze the avalanches of directed sandpile models on the Apollonian network. We make use of the properties of this specific network and model to first derive a series of exact results for the distribution of avalanches. Then, these results can be extended, with the help of the numerical iteration of the obtained recurrence relations, to illustrate more general situations. More precisely, we are able to investigate the fine details of the local mass flux, deriving the appropriate multifractal spectra that describe the scaling properties of the flux.

This work is organized as follows: In Sec. II we introduce our model, discussing the role played by the number of levels, q , in the Apollonian hierarchy that limit which nodes can receive mass from a toppling neighbor. We also derive the basic expressions for the two- and three-point correlation functions that allow for the derivation of the local and total fluxes. Results for the total flux, obtained by numerical iteration, are discussed in Sec. III, for $1 \leq q \leq 6$. They are then compared with analytical expressions derived for the $q=1$ and $q=2$. In Sec. IV, a multifractal approach is used to present the scaling properties of the flux for the distinct values of q . Finally, Sec. V closes the paper with our concluding remarks.

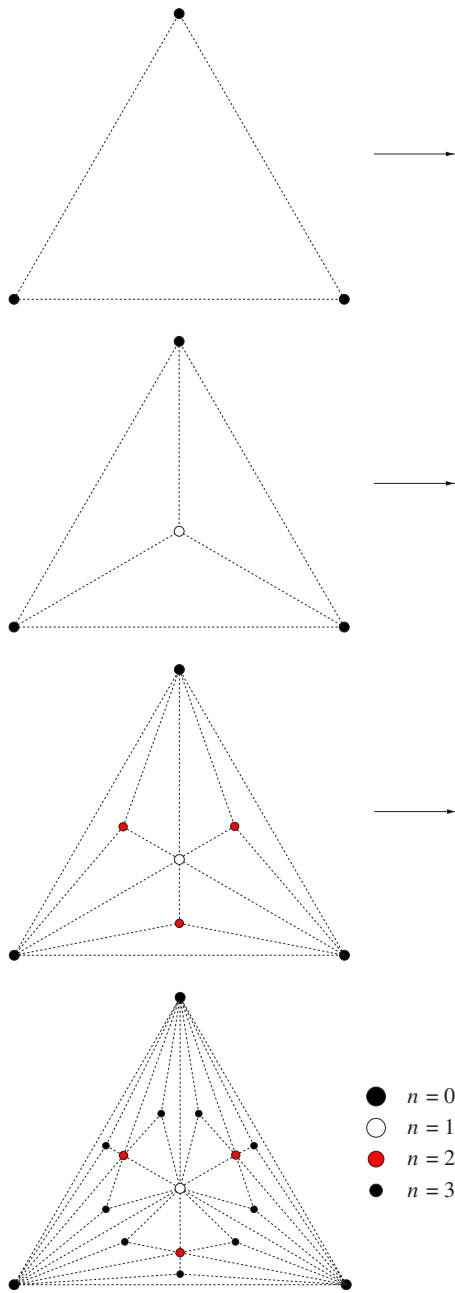


FIG. 1. (Color online) Building process of the Apollonian network.

II. DIRECTED SANDPILE MODELS ON THE APOLLONIAN NETWORK

The planar Apollonian network [17] is obtained from the classical Apollonian space-filling packing of circles [20] by associating nodes with the centers of the circles and drawing edges between nodes corresponding to pairs of touching circles. This iterative building process is illustrated in Fig. 1.

The directed sandpile model of Dhar and Ramaswamy [15] associates with each site \mathbf{x} of a hypercubic lattice a height variable $z(\mathbf{x})$, which is increased by one when a grain is added to \mathbf{x} . If $z(\mathbf{x})$ exceeds a critical value z_c , the site topples and the height variables at all ℓ nearest neighbors of \mathbf{x} along a preferred direction increase by 1, while $z(\mathbf{x})$ de-

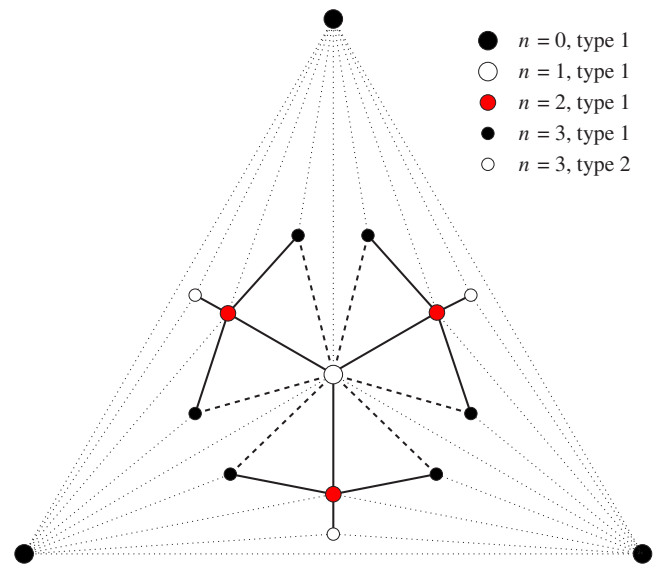


FIG. 2. (Color online) Apollonian network with $q=2$. Dotted lines correspond to inactive connections and thick lines indicate connections between sites in adjacent layers, while dashed lines connect sites separated by two layers. Note that there are two types of sites in layer $n=3$. If $q=1$, also dashed lines become inactive.

creases by ℓ . In order to satisfy this requirement, we must have $z_c \geq \ell$; without loss of generality, we assume that $z_c = \ell$. Notice that, once a site \mathbf{x} receives its first grain, its height variable cannot return to the value $z(\mathbf{x})=0$. Configurations of the lattice in which all height variables assume values between 1 and z_c are called stable.

The model is driven by the addition of grains to randomly chosen sites. If the chosen site topples, an avalanche is initiated, stopping after no additional topplings can occur. Then, a grain is added to another randomly chosen site. After a sufficiently large number of grain additions, the system reaches a SOC state, in which avalanches connect stable configurations.

The existence of a preferred direction is essential to the exact solvability of the model, not only in its original form but also in generalized versions [21]. In the Apollonian network, the building process offers an obvious choice of a preferred direction. We define the n th layer of the network as the set of sites added in the n th iteration of the process, and we postulate that, when a site in a given layer topples, only sites in subsequent layers can receive grains. However, the Apollonian network has the peculiar property that each site in a given layer is connected to at least one site in each subsequent layer. Thus, in the thermodynamic limit, any site has an infinite number of neighbors in subsequent layers, leading to an infinite critical height. In order to obtain a finite value of z_c , we impose the restriction that only neighbors in the first q subsequent layers can receive grains when a site topples, the remaining connections being inactive; see Fig. 2. This leads to a q -dependent value of the critical height z_c , which is the same for all sites in the network, provided we forbid the addition of grains to the sites in the original triangle (layer $n=0$). (For q from 1 to 6, we have $z_c=3, 9, 21, 45, 93$, and 189.) Thus, all allowed sites have an equivalent set of neighbors in their subsequent layers, and we can study

the properties of avalanches by choosing any reference site \mathbf{x}_0 . For convenience, we choose \mathbf{x}_0 to be the site located at the geometrical center of the network (layer $n=1$). As we show later on, by working with finite values of q it is possible to infer the behavior of the system in the $q \rightarrow \infty$ limit.

As in the original directed sandpile model, we define a two-point correlation function $G_0(\mathbf{x}; \mathbf{x}_0)$ which measures the probability that a site \mathbf{x} topples in the SOC state due to an avalanche originated by adding a grain at \mathbf{x}_0 . Due to the fact that all stable configurations are equally probable in the SOC state [15] and that all allowed sites have an equivalent set of neighbors, the probability that a site topples, provided that r of its backwards neighbors have toppled, is equal to r/z_c . Thus, G_0 obeys the recursion equation

$$G_0(\mathbf{x}; \mathbf{x}_0) = \frac{1}{z_c} \left[\sum_{\mathbf{y}}' G_0(\mathbf{y}; \mathbf{x}_0) + \delta_{\mathbf{x}, \mathbf{x}_0} \right], \quad (1)$$

with the primed summation running over all sites from which \mathbf{x} can receive grains, according to the q -layer rule. Since

$$G_0(\mathbf{x}_0; \mathbf{x}_0) = \frac{1}{z_c}, \quad (2)$$

the existence of a preferred direction allows us to solve Eq. (1) for all $G_0(\mathbf{x}; \mathbf{x}_0)$, at least numerically.

The flux through the n th layer is given by

$$\phi(n) = \sum_{\mathbf{x} \in n} G_0(\mathbf{x}; \mathbf{x}_0). \quad (3)$$

Contrary to what is observed in hypercubic lattices, here $\phi(n)$ generally depends on n , although it becomes asymptotically constant for $n \gg 1$, as we show below by numerical and analytical calculations. If $m(n)$ is the average number of sites in the n th layer that topple when at least one of them does, we can write

$$\phi(n) = m(n)p(n), \quad (4)$$

in which $p(n)$ is the probability that, in the SOC state, an avalanche started at \mathbf{x}_0 reaches layer n .

If we assume that

$$p(n) \sim n^{-\alpha}, \quad (5)$$

with some exponent α , the asymptotic constancy of $\phi(n)$ allows us to conclude that

$$m(n) \sim \frac{1}{p(n)} \sim n^\alpha. \quad (6)$$

Thus, the average mass of an avalanche reaching at least n layers scales as

$$M(n) = \sum_{t=1}^n m(t) \sim \int_1^n dt t^\alpha \sim n^{\alpha+1}, \quad (7)$$

and the probability that the total mass of an avalanche exceeds M can be written as

$$\hat{p}(M) = p(n(M)) \sim M^{-\alpha/(1+\alpha)}. \quad (8)$$

Finally, we obtain for $\rho(M)$, the probability distribution of avalanches with size M ,

$$\rho(M) = \frac{d\hat{p}(M)}{dM} \sim M^{-(1+2\alpha)/(1+\alpha)} \equiv M^{-\tau}. \quad (9)$$

The exponent α can be calculated from the mean-square flux

$$\Phi(n) \sim [m(n)]^2 p(n) \sim n^\alpha, \quad (10)$$

which is related to the three-point correlation function $G(\mathbf{x}_1, \mathbf{x}_2; \mathbf{x}_0)$, defined as the probability that sites \mathbf{x}_1 and \mathbf{x}_2 , both in the same layer, topple due to an avalanche started by adding a grain at site \mathbf{x}_0 . Explicitly, we have

$$\Phi(n) = \sum_{\mathbf{x}_1, \mathbf{x}_2 \in n} G(\mathbf{x}_1, \mathbf{x}_2; \mathbf{x}_0). \quad (11)$$

As in the case of $G_0(\mathbf{x}; \mathbf{x}_0)$, we can write for $G(\mathbf{x}_1, \mathbf{x}_2; \mathbf{x}_0)$ a recursion equation

$$G(\mathbf{x}_1, \mathbf{x}_2; \mathbf{x}_0) = \frac{1}{z_c^2} \sum_{\mathbf{y}_1, \mathbf{y}_2}' G(\mathbf{y}_1, \mathbf{y}_2; \mathbf{x}_0), \quad (12)$$

with the primed summation running over all sites from which \mathbf{x}_1 or \mathbf{x}_2 can receive grains, according to the q -layer rule. This last equation can be solved by the ansatz [22,23]

$$G(\mathbf{x}_1, \mathbf{x}_2; \mathbf{x}_0) = \sum_{\mathbf{y}} f(\mathbf{y}; \mathbf{x}_0) G_0(\mathbf{x}_1; \mathbf{y}) G_0(\mathbf{x}_2; \mathbf{y}), \quad (13)$$

with the function $f(\mathbf{y}; \mathbf{x}_0)$ determined by the condition

$$G(\mathbf{x}, \mathbf{x}; \mathbf{x}_0) = G_0(\mathbf{x}; \mathbf{x}_0), \quad (14)$$

which leads to

$$\sum_{\mathbf{y}} f(\mathbf{y}; \mathbf{x}_0) G_0(\mathbf{x}; \mathbf{y}) G_0(\mathbf{x}; \mathbf{y}) = G_0(\mathbf{x}; \mathbf{x}_0). \quad (15)$$

Summing over all sites \mathbf{x} in the same layer n , using Eq. (3) and the fact that $G(\mathbf{x}; \mathbf{y}) = G(\mathbf{x} - \mathbf{y} + \mathbf{x}_0; \mathbf{x}_0)$, we can rewrite Eq. (15) as

$$\sum_{t=1}^n F(t) K(n-t+1) = \phi(n), \quad (16)$$

in which

$$F(t) = \sum_{\mathbf{y} \in t} f(\mathbf{y}), \quad K(t) = \sum_{\mathbf{x} \in t} G_0(\mathbf{x}; \mathbf{x}_0) G_0(\mathbf{x}; \mathbf{x}_0). \quad (17)$$

Starting from $n=1$, Eq. (16) can be solved recursively for $F(n)$. By substituting Eq. (13) into Eq. (11), we can express $\Phi(n)$ in terms of $F(n)$,

$$\Phi(n) = \sum_{t=1}^n F(t) [\phi(n-t+1)]^2. \quad (18)$$

The scaling behavior of $\Phi(n)$ determines the exponent α .

The case $q=1$ is immediately solved. In this limit, the Apollonian network (with the three original vertices removed) reduces to a Cayley tree with coordination number equal to 4, as shown in Fig. 2. The two-point correlation is easily seen to satisfy

$$G_0(\mathbf{x}; \mathbf{x}_0) = \frac{1}{3^n}, \quad \mathbf{x} \in n, \quad (19)$$

so that the average flux is $\phi(n) = 1/3$, $\forall n$, leading to

$$K(n) = \frac{1}{3^{n+1}}, \quad F(1) = 3, \quad F(n) = 2 \quad (n > 1). \quad (20)$$

Thus, the mean-square flux is given by

$$\Phi(n) = \frac{1}{9} + \frac{2}{9}n, \quad (21)$$

corresponding to $\alpha=1$ ($\tau=3/2$), characteristic of the mean-field behavior associated with the directed model in Bravais lattices with dimension $d \geq 4$. For the purpose of comparison, the corresponding exact values in $d=2$ are $\alpha=1/2$, $\tau=4/3$.

In the next two sections, we discuss the properties of the model for $q > 1$.

III. AVERAGE BEHAVIOR

For $q \geq 2$, sites in the same layer are no longer equivalent, since we are preserving the underlying topology of the Apollonian network as defined by the building rule. Instead, those sites are naturally grouped in different classes, defined by the structure of their connection to sites in previous layers. In principle, this makes the model amenable to analytical treatment. As we show in the Appendix, the analysis for $q=2$ is already somewhat intricate, but it lends support to a series of conclusions we obtain from numerical calculations. These are performed by building an Apollonian network with up to 16 layers (corresponding to 21 523 363 sites), imposing the q -layer rule, and solving recursively Eqs. (1) and (16). From this, we can calculate both the mean flux $\phi(n)$ and the mean-square flux $\Phi(n)$ as functions of the layer index n . (In Sec. IV we study the local properties of the flux.)

The first conclusion to emerge from our numerical analysis is that the mean flux $\phi(n)$ becomes asymptotically constant for large n , as already mentioned in Sec. II. This is evident in Fig. 3(a), where we plot, for several values of q , the ratio between $\phi(n)$ and the corresponding (constant) result for $q=1$. Notice the oscillations in $\phi(n)$ for small values of n . These are related to the fact that, as the number of neighbors of a site in a given subsequent layer increases with the layer index, so does the fraction of grains received by each layer when the site topples. Owing to the q -layer rule, for $q > 1$, the mean flux reaching layer $n=2$ drops in comparison with the total flux, then increases from $n=2$ to $n=q+1$, dropping again for $n=q+2$. But this second drop is smaller, because sites in that layer receive grains from all q previous layers. As a result of this process, the oscillations are smoothed out for sufficiently high values of n .

Corresponding curves for the mean-square flux are shown in Fig. 3(b). Again the curves oscillate for small values of the layer index n , but approach a constant value for large n , showing that $\Phi(n)$ always satisfies the asymptotic scaling form

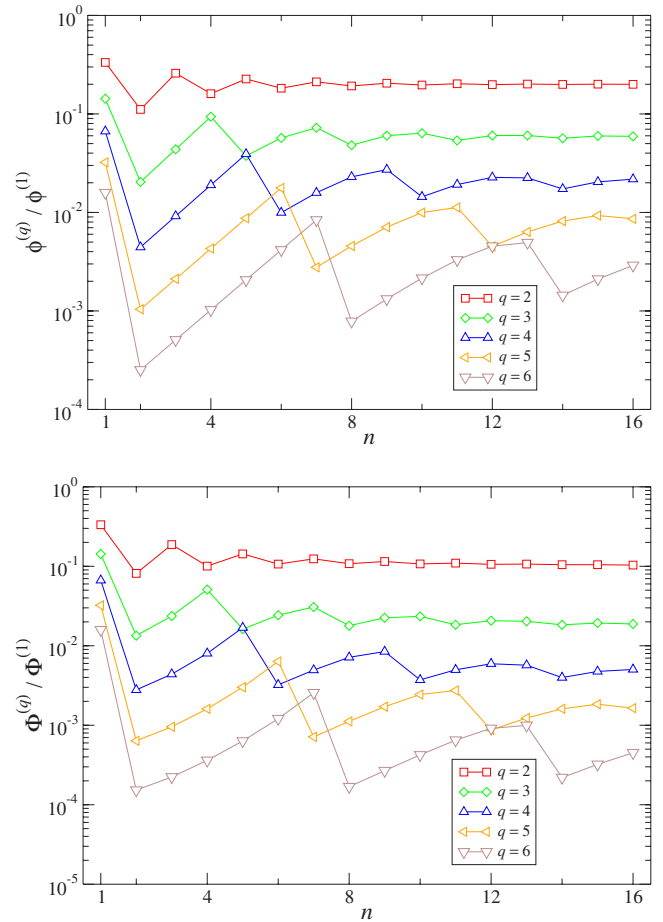


FIG. 3. (Color online) (a) Mean flux as a function of the layer index n , for different values of q , divided by the mean flux for $q=1$. (b) Corresponding curves for the mean-square flux.

$$\Phi(n) \sim n. \quad (22)$$

This means that, if we fix q and let $n \rightarrow \infty$, the distribution of avalanche sizes follows, asymptotically, a power law with exponent $\alpha=1$, irrespective of q .

On the other hand, the model behaves differently if we consider the condition in which $q \rightarrow \infty$, corresponding to the genuine Apollonian network model. To analyze this situation, let us observe what happens at smaller scales in the finite- q -layer rule. As clearly shown in Fig. 3(a), $\phi(n)$ depends exponentially on n between $n=2$ and $n=q+1$,

$$\phi(n) = A e^{an}, \quad (23)$$

with a q -dependent prefactor A , but a nearly constant value of $a \approx 0.7$. The prefactor A decreases exponentially with q , since it is related to the inverse threshold height $1/z_c$. The exponential (rather than linear) dependence of $\phi(n)$ is a consequence of the exponential increase in the number of neighbors as a function of the layer separation. In the $q \rightarrow \infty$ limit, the central site topples only after the addition of an enormous number of grains, most of which are then received by sites in very distant layers. As a consequence, all avalanches have arbitrarily large range. In this case, the exponent α formally takes an infinite value.

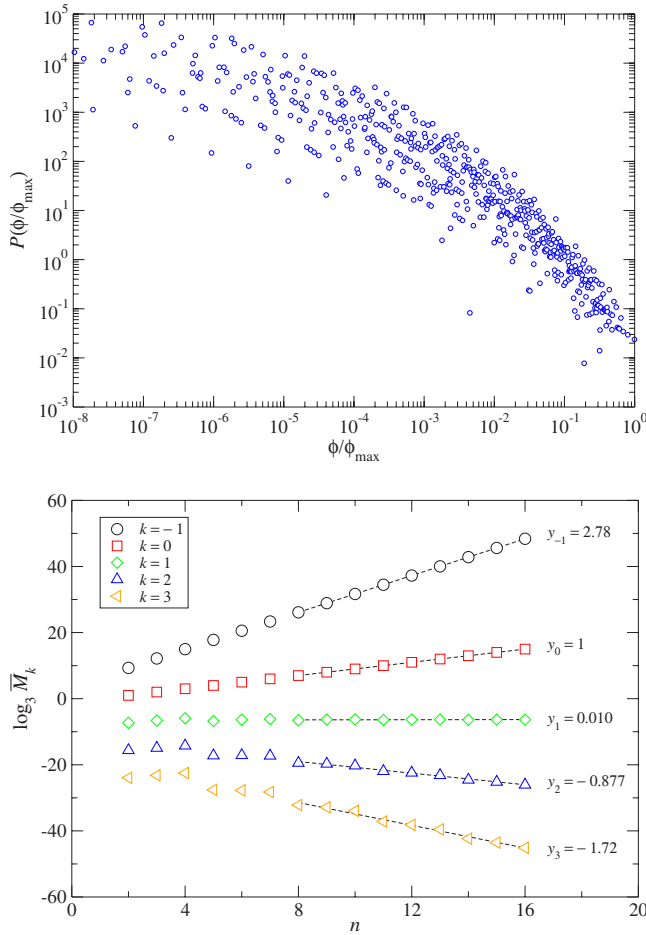


FIG. 4. (Color online) (a) Flux distributions in a given layer, rescaled by the corresponding maximum flux, for $q=2$ and $n=22$. (b) Moments of the flux as a function of n , for $q=3$ and several values of k , with the corresponding exponents y_k .

We conclude this analysis with the observation that the model offers different asymptotic behaviors, depending on the finite or infinite character of q . If $q \rightarrow \infty$, the asymptotic behavior does not fit into the usual SOC framework. If q is finite, we observe the prevalence of a mean-field behavior, which could be anticipated on the basis of the treelike topology of the lattice obtained by imposing the q -layer rule. A similar situation arises in other sandpile models on different forms of decorated Cayley trees [23,24]; since the correlation length is infinite in the SOC state, the mean-field behavior characteristic of the ordinary Cayley tree (or more precisely the Bethe lattice) is recovered.

IV. MULTIFRACTAL PROPERTIES OF THE FLUX

Although the average behavior of the flux reproduces that of the mean-field limit for finite values of q , the local-flux distribution reveals interesting properties already for $q=2$. In Fig. 4(a) we plot histograms of the local flux ϕ for $n=22$ (plots for $n=20$ or $n=21$ give statistically equivalent results). Owing to a precise identification of the distinct types of sites for the $q=2$ model, we were able to consider a much larger number of nodes ($>10^{10}$) than for the results reported in the

previous section. The fluxes are rescaled by the corresponding maximum flux ϕ_{\max} in that layer. The many discontinuities in the histogram are due to the fact that the local fluxes in a given layer assume only a set of discrete values, clustered around powers of z_c^{-1} . Note that there are very few sites with large local fluxes, while the local flux through the vast majority of sites is very small. This leads to an appreciable difference between average and typical behavior.

In analogy with studies of the distribution of currents in the incipient infinite cluster of a random-resistor network [25], it is interesting to evaluate the moments of the flux in order to better reveal the scaling properties hidden in Fig. 4(a). So we use the definition

$$\bar{M}_k(n) = \sum_{\mathbf{x} \in n} \left(\frac{\phi_{\mathbf{x}}}{\phi_0} \right)^k, \quad (24)$$

in which the summation runs over all sites \mathbf{x} in the n th layer of the Apollonian network,

$$\phi_{\mathbf{x}} \equiv G_0(\mathbf{x}; \mathbf{x}_0), \quad (25)$$

and ϕ_0 is the initial flux. It turns out that, for all real values of k , the moments satisfy scaling relations given by

$$\bar{M}_k(n) \sim e^{u_k n}, \quad (26)$$

with well-defined coefficients u_k , so that, in terms of the system size

$$L \sim 3^{n+1}, \quad (27)$$

we have

$$\bar{M}_k(L) \sim L^{y_k}, \quad (28)$$

with $y_k = u_k / \ln 3$. For $q=1$, all sites in a given layer n have the same flux 3^{-n} , so that the exponents y_k are given by $y_k = 1 - k$. For $q \geq 2$, on the other hand, we see from our numerical calculations that there is no simple linear relation between the exponents y_k , suggesting that no single number characterizes the current distribution. This is a signature of multifractal behavior. A plot of $\bar{M}_k(n)$ for $q=3$ and several values of k is shown in Fig. 4(b).

To further investigate the multifractal properties of the flux distribution, we evaluate the dependence of y_k with respect to k , as well as the multifractal spectrum $f(\bar{\alpha})$, defined by a Legendre transform of the exponents y_k ,

$$f(\bar{\alpha}) = y_k + k\bar{\alpha}, \quad \bar{\alpha} = -\frac{dy_k}{dk}. \quad (29)$$

Figure 5 shows plots of y_k versus k for different values of k . These plots were obtained by calculating the moments \bar{M}_k as functions of the layer index n for 300 values of k between -10 and 10 , and then extracting the exponents y_k by least-squares power-law fits of \bar{M}_k between $n=n_1$ and $n=n_2$. For $q=2$, the resulting curves show a very weak dependence on the values of n_1 and n_2 ; specifically, fixing $n_1=5$ or $n_1=10$ and varying n_2 between $n=18$ and $n=22$ leads to a relative error of the order of 10^{-5} around $k=0$. Notice that, for values of k approximately between -1 and 1 , an extended crossover

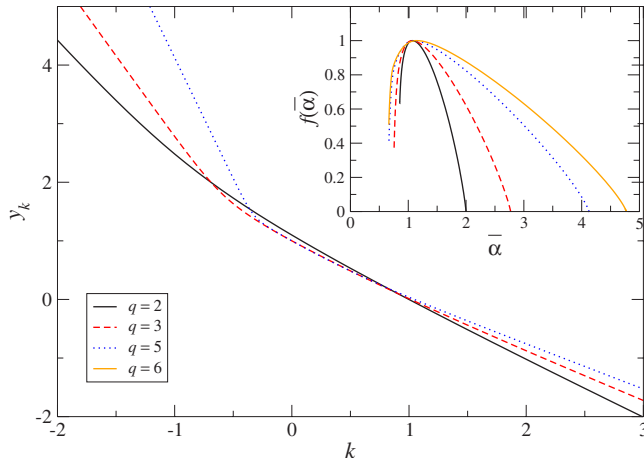


FIG. 5. (Color online) Plots of the exponents y_k versus k for $q=2, 3$, and 5 . Inset: plots of $f(\bar{\alpha})$ for $q=2, 3, 5$, and 6 .

separating two distinct linear regimes is clear in Fig. 5. From the log-log plot in Fig. 4(a), we conclude that one linear regime corresponds to large negative values of k , in which the moments \bar{M}_k are dominated by a huge number of sites with very low fluxes, while the other regime is produced by large positive values of k , in which \bar{M}_k is determined by a tiny number of sites with large fluxes. This is a similar mechanism to the one producing multifractality in the square-lattice Abelian sandpile model [26], which is associated with the dominance of rare, very large avalanches.

Plots of $f(\bar{\alpha})$ for several values of q are shown in the inset of Fig. 5. Note that, according to Eq. (29), the maximum of $f(\bar{\alpha})$ occurs for the value of α associated with $k=0$, for which $f(\bar{\alpha}_{k=0})=y_0$. Indeed, for $q=1$ (not shown in Fig. 5), the curve consists of a single point $(\bar{\alpha}_{k=0}, y_0)=(1, 1)$, corresponding to a monofractal behavior. Within numerical errors, that point is the maximum of all curves, in agreement with the fact that $y_0=1$ for all values of q .

For $q \geq 2$, the left (right) end of the curves reflects the scaling behavior of the set of points associated with the largest (smallest) fluxes. Although not visible in the plots, the density of points is much larger near the ends of the curves, with intermediate points coming mostly from values of k between -1 and 1 . The width of the curves increases with q , presumably diverging as $q \rightarrow \infty$. This is related to the fact that larger values of q lead to a larger range of values of the flux in each layer of the lattice.

V. CONCLUSIONS

In this work we investigated directed sandpile models on the Apollonian network, subject to a rule stating that, when a site topples, only sites in the first q subsequent layers can receive grains. Analytical results were obtained for the avalanche probability distribution when $q=1$ and 2 , while larger values of q were studied by numerical evaluation of analytical expressions. For finite values of q , the avalanche distributions follow asymptotic power-law scaling forms, with typical mean-field exponents, since the q -layer rule effec-

tively constrains the Apollonian network to a tree structure. On the other hand, our results also show the emergence of large oscillatory deviations due to finite- q effects, suggesting that, in the $q \rightarrow \infty$ limit, corresponding to the genuine Apollonian network, an exponential dependence of the average flux with the layer index is obtained.

Investigation of the local properties of the fluxes through each node showed that the network topology induces a large degree of inhomogeneity in the sandpile model for $q \geq 2$, giving rise to multifractal scaling. The origin of the multifractality lies in the presence of a very small number of sites experiencing a large fraction of the average flux. A similar effect has been observed in simulations for the Abelian sandpile model in the square lattice [26], in which rare, large avalanches dominate the statistics.

Finally, the comparison with results found for another sandpile model on scale-free networks [10] shows similarities in the mean-field behavior when all nodes share the same critical height or the critical height depends locally on the node degree.

ACKNOWLEDGMENTS

This work was partially financed by the Brazilian agencies CNPq, FUNCAP, and FAPESB. H.J.H. acknowledges the support of the Max Planck prize.

APPENDIX: ANALYTICAL TREATMENT FOR $q=2$

For $q \geq 2$, the sites in each layer of the Apollonian network can be grouped into types according to how they are connected to their backwards neighbors. This feature can be exploited in order to obtain analytical results for the behavior of the directed sandpile model. Here we deal with the case $q=2$, which allows us to check our numerical results in a reasonably simple way. It is clear that the treatment can be extended to higher values of q , with basically the same results, but a considerably larger amount of work.

Layer $n=1$ of the network contains only one site, while the three sites in layer $n=2$ are all equivalent. However, already for $n=3$ two types of sites are present: sites of type 1 receive grains from sites in the two previous layers, while sites of type 2 receive grains only from the latter layer; see Fig. 2. For $n=4$, two additional types of sites would appear, since it is possible that a site receives grains from sites of type 1 or 2, in one or two of the previous layers. It is easy to convince oneself that the number of site types doubles for each additional layer (starting at $n=2$) and that the types can be labeled so that each site of type s has as nearest neighbors in the next layer two sites of type $2s-1$ and one site of type $2s$.

Denoting by $g_{n,s}$ the value of $G_0(\mathbf{x}; \mathbf{x}_0)$ for a site \mathbf{x} of type s in layer n and by $\nu_{n,s}$ the number of such sites, the flux through layer n can be written as

$$\phi(n) = \sum_{s=1}^{2^{n-2}} \nu_{n,s} g_{n,s}. \quad (\text{A1})$$

In order to estimate $\phi(n)$, we must investigate the asymptotic behavior of both $\nu_{n,s}$ and $g_{n,s}$.

Our choice of labels allows us to write, for $s=2j-1$ ($j=1,2,3,\dots$),

$$g_{n,2j-1} = \frac{1}{9}(g_{n-1,j} + g_{n-2,(j+1)/2}), \quad \nu_{n,2j-1} = 2\nu_{n-1,j}, \quad (\text{A2})$$

in which $[w]$ denotes the integer part of the number w and, for $s=2j$,

$$g_{n,2j} = \frac{1}{9}g_{n-1,j}, \quad \nu_{n,2j} = \nu_{n-1,j}. \quad (\text{A3})$$

Equations (A2) and (A3), being recursive expressions, can be solved numerically to yield all $g_{n,s}$ and $\nu_{n,s}$ in terms of $g_{1,1}$ and $\nu_{1,1}$. However, analytical results can be derived from the observation that $g_{n,1}$ behaves as

$$g_{n,1} \sim \zeta^n, \quad (\text{A4})$$

with $\zeta = (1 + \sqrt{37})/18 \approx 0.393$ being determined from the solution of the equation

$$\zeta^2 = \frac{1}{9}(\zeta + 1). \quad (\text{A5})$$

Consequently, $g_{n,s}$ satisfies

$$g_{n,s} \approx A_s \zeta^n, \quad (\text{A6})$$

with constant prefactors A_s . Moreover, the multiplicities $\nu_{n,s}$ are such that $\nu_{n,1} = 3 \times 2^{n-2}$ ($n \geq 2$) and the ratios $f_s \equiv \nu_{n,s}/\nu_{n,1}$ satisfy

$$f_{2j-1} = \frac{\nu_{n,2j-1}}{\nu_{n,1}} = \frac{2\nu_{n,j}}{2\nu_{n,1}} = f_j, \quad (\text{A7})$$

$$f_{2j} = \frac{\nu_{n,2j}}{\nu_{n,1}} = \frac{\nu_{n,j}}{2\nu_{n,1}} = \frac{1}{2}f_j.$$

We can rewrite Eq. (A1) as

$$\phi(n) = \nu_{n,1} \sum_{s=1}^{2^{n-2}} f_s g_{n,s} = \nu_{n,1} \sum_{m=0}^{n-2} \Gamma_{n,m}, \quad (\text{A8})$$

with

$$\Gamma_{n,0} = g_{n,1}, \quad \Gamma_{n,m} = \sum_{s=1+2^{m-1}}^{2^m} f_s g_{n,s} \quad (m \geq 1). \quad (\text{A9})$$

Making use of the definition of $\Gamma_{n,m}$ and of Eqs. (A2), (A3), and (A7), we can obtain the recursion equation

$$\Gamma_{n,m} = \frac{1}{6}(\Gamma_{n-2,m-2} + \Gamma_{n-1,m-1}). \quad (\text{A10})$$

Keeping in mind Eq. (A6), we expect that $\Gamma_{n,m}$ takes the asymptotic form

$$\Gamma_{n,m} \approx \gamma_m \zeta^n. \quad (\text{A11})$$

Substituting this last expression into Eq. (A10), we conclude that the constants γ_m satisfy the equation

$$\gamma_m \zeta^2 - \frac{1}{6} \gamma_{m-1} \zeta - \frac{1}{6} \gamma_{m-2} = 0, \quad (\text{A12})$$

which can be solved by $\gamma_m \approx \gamma_0 \theta^m$, with $\theta = (2\zeta)^{-1}$. We then have

$$\Gamma_{n,m} \sim \theta^n \zeta^n = \frac{1}{2^m} \zeta^{n-m}, \quad (\text{A13})$$

and the flux $\phi(n)$ scales with the layer index as

$$\phi(n) \sim 2^n \cdot \zeta^n \sum_{m=0}^{n-2} \theta^m = (2\zeta)^n \frac{\theta^{n-1} - 1}{\theta - 1}. \quad (\text{A14})$$

Since $\theta > 1$, this is equivalent to

$$\phi(n) \sim (2\zeta\theta)^n = 1, \quad (\text{A15})$$

so that the flux becomes asymptotically constant for $n \gg 1$.

The function $K(n)$, defined by

$$K(n) = \sum_{\mathbf{x} \in n} G_0(\mathbf{x}; \mathbf{x}_0) G_0(\mathbf{x}; \mathbf{x}_0) = \sum_{s=1}^{2^{n-2}} \nu_{n,s} g_{n,s}^2, \quad (\text{A16})$$

scales as $K(n) \sim \zeta^n$ and thus vanishes exponentially for large n . In the same limit, the function $F(n)$, related to $K(n)$ and $\phi(n)$ through the equation

$$\sum_{t=1}^n F(t) K(n-t+1) = \phi(n), \quad (\text{A17})$$

tends to a constant value. As a consequence, the mean-square flux must scale as

$$\Phi(n) = \sum_{t=1}^n F(n)[\phi(n-t+1)]^2 \sim n, \quad (\text{A18})$$

yielding the mean-field exponent $\alpha=1$.

- [1] R. Albert and A. L. Barabasi, Rev. Mod. Phys. **74**, 47 (2002).
 [2] L. N. A. Amaral, A. Scala, M. Barthelemy, and H. E. Stanley, Proc. Natl. Acad. Sci. U.S.A. **97**, 11149 (2000).
 [3] S. Boccaletti, V. Latora, Y. Moreno, M. Chavez, and D. U. Hwang, Phys. Rep. **424**, 175 (2006).

- [4] R. Pastor-Satorras, A. Vazquez, and A. Vespignani, Phys. Rev. Lett. **87**, 258701 (2001).
 [5] A. Aleksiejuka, J. Holyst, and D. Stauffer, Physica A **310**, 260 (2002).
 [6] S. N. Dorogovtsev, A. V. Goltsev, and J. F. F. Mendes, Eur.

- Phys. J. B **38**, 177 (2004).
- [7] M. Bauer, S. Coulomb, and S. N. Dorogovtsev, Phys. Rev. Lett. **94**, 200602 (2005).
- [8] B. Kramer, T. Ohtsuki, and S. Kettemann, Phys. Rep. **417**, 211 (2005).
- [9] P. Bak, C. Tang, and K. Wiesenfeld, Phys. Rev. Lett. **59**, 381 (1987).
- [10] K.-I. Goh, D.-S. Lee, B. Kahng, and D. Kim, Phys. Rev. Lett. **91**, 148701 (2003).
- [11] G. Bianconi and M. Marsili, Phys. Rev. E **70**, 035105(R) (2004).
- [12] L. de Arcangelis, C. Perrone-Capano, and H. J. Herrmann, Phys. Rev. Lett. **96**, 028107 (2006).
- [13] C.-W. Shin and S. Kim, Phys. Rev. E **74**, 045101(R) (2006).
- [14] G. L. Pellegrini, L. de Arcangelis, H. J. Herrmann, and C. Perrone-Capano (unpublished).
- [15] D. Dhar and R. Ramaswamy, Phys. Rev. Lett. **63**, 1659 (1989).
- [16] H. J. Herrmann, G. Mantica, and D. Bessis, Phys. Rev. Lett. **65**, 3223 (1990).
- [17] J. S. Andrade, H. J. Herrmann, R. F. S. Andrade, and L. R. da Silva, Phys. Rev. Lett. **94**, 018702 (2005).
- [18] J. P. K. Doye and C. P. Massen, Phys. Rev. E **71**, 016128 (2005).
- [19] R. F. S. Andrade and H. J. Herrmann, Phys. Rev. E **71**, 056131 (2005).
- [20] D. W. Boyd, Can. J. Math. **25**, 303 (1973).
- [21] R. F. S. Andrade, Braz. J. Phys. **33**, 437 (2003).
- [22] D. Dhar, Phys. Rev. Lett. **64**, 1613 (1990).
- [23] D. Dhar and S. N. Majumdar, J. Phys. A **23**, 4333 (1990).
- [24] V. V. Papoyan and R. R. Shcherbakov, J. Phys. A **28**, 6099 (1995).
- [25] D. Stauffer and A. Aharony, *Introduction to Percolation Theory*, 2nd ed. (Taylor & Francis, London, 2003).
- [26] M. De Menech, A. L. Stella, and C. Tebaldi, Phys. Rev. E **58**, R2677 (1998).